HHS Public Access
Author manuscript
Cell Signal. Author manuscript; available in PMC 2016 February 08.

Published in final edited form as:
Cell Signal. 2014 May ; 26(5): 1135–1146. doi:10.1016/j.cellsig.2014.01.009.

A new non-canonical pathway of Gα_q protein regulating mitochondrial dynamics and bioenergetics

Cristiane Benincá[1,3], **Jesús Planagumà**[2], **Adriana de Freitas Shuck**[1], **Rebeca Acín-Perez**[3], **Juan Pablo Muñoz**[4], **Marina Mateus de Almeida**[5], **Joan H. Brown**[6], **Anne N. Murphy**[6], **Antonio Zorzano**[4], **Jose Antonio Enríquez**[3], and **Anna M. Aragay**[1,2,*]

[1]Molecular Biology Institute of Barcelona (IBMB), Spanish National Research Council (CSIC), Barcelona 08028, Spain

[2]Department of Biomedicine, University of Bergen, 5009 Bergen, Norway

[3]Department of Cardiovascular Development and Repair, Spanish Cardiovascular Research Center (CNIC), Madrid 28029, Spain

[4]Institute for Research in Biomedicine (IRB), Barcelona 08028, Spain; Departament de Bioquímica i Biologia Molecular, Universitat de Barcelona; and CIBERDEM

[5]Department of Genetics, Federal University of Paraná (UFPR), Curitiba PO Box 19071, Brazil

[6]Department of Pharmacology, University of California (UCSD), San Diego CA92093-0636, USA

Abstract

Contrary to previous assumptions, G proteins do not permanently reside on the plasma membrane, but are constantly monitoring the cytoplasmic surfaces of the plasma membrane and endomembranes. Here, we report that the Gα_q and Gα_{11} proteins locate at the mitochondria and play a role in a complex signaling pathway that regulates mitochondria dynamics. Our results provide evidence for the presence of the heteromeric G protein (G$\alpha_{q/11}\beta\gamma$) at the outer mitochondrial membrane and for Gα_q at the inner membrane. Both localizations are necessary to maintain the proper equilibrium between fusion and fission; which is achieved by altering the activity of mitofusin proteins, Drp1, OPA1 and the membrane potential at both the outer and inner mitochondrial membranes. As a result of the absence of G$\alpha_{q/11}$, there is a decrease in mitochondrial fusion rates and a decrease in overall respiratory capacity, ATP production and OXPHOS-dependent growth. These findings demonstrate that the presence of Gα_q proteins at the mitochondria serves a physiological function: stabilizing elongated mitochondria and regulating energy production in a Drp1 and Opa1 dependent mechanisms. This thereby links organelle dynamics and physiology.

*Correspondence and request for materials should be addressed to: A.M.A. (aarbmc@ibmb.csic.es).

Author contributions

CB designed the experiments and was involved in most of the mitochondrial and microscopy analysis; CB and JP analyzed the microscopy data; AdeFS cloned and analyzed the Gα_q chimeras; CB and JPM performed the ATP and TMR measurements; RAP and CB prepared the supercomplexes and carried out the OCR analysis; MMdeA performed the statistical analysis; AM analyzed the mitochondrial subcompartments; JHB, AZ, JAI and AA contributed to the design of the experiments; CB and AA wrote the manuscript with input from all the authors.

Introduction

Heterotrimeric G proteins, consisting of an α subunit and a complex formed of β γ subunits, are well-established mediators of signal transduction pathways downstream from G protein-coupled receptors (GPCRs). For many years it was believed that G proteins perform their function at or close to the plasma membrane. Only recently did it become evident that G proteins can be localized at and signal to different endomembranes, including the endoplasmic reticulum (ER) and Golgi, and that their localization can be highly dynamic [1]. Recent findings have identified the mitochondria as a non-canonical localization for G proteins, including $G\alpha_{12}$ [2], $G\alpha_i$ [3] and Gβ2 [4]. Moreover, recent reports confirm that some G protein-effectors or binding partners, such as MAPKs, Akt, GRK2 and PKC, are also present at the mitochondria; particularly at the outer mitochondrial membrane and in the intermembrane space [5, 6], which suggests that this new localization of G proteins may be functionally important.

Of the different types of Gα, the $G\alpha_q$ family members (including $G\alpha_q$, $G\alpha_{11}$, $G\alpha_{14}$ and $G\alpha_{15/16}$) [7] stimulate the β-isoform of phosphoinositide phospholipase C (PLC-β), which in turn increases inositol lipid (i.e., calcium/PKC) signaling [8]. The members of the human Gq family, $G\alpha_{11}$, $G\alpha_{14}$ and $G\alpha_{16}$, share approximately 90%, 80% and 57% homology, respectively, of their amino acid sequence with $G\alpha_q$ [7]. Most downstream cellular responses result from enhanced calcium signaling, but growing evidence indicates that other events may account for some of the physiological roles of $G\alpha_q$ family members [8]. A growing list of scaffolding/adaptor proteins (caveolin-1 [9], EBP50/NHERF1 [10], CD9/CD81 [11], Flotilin [12], TRP1 [13]), regulatory proteins (RGS [14, 15]), GRKs [16, 17], effectors (RhoGEFs [18], Btk [19], PKCζ/ERK5 [20]) and activator proteins (Ric-8A [21], tubulin [22]) may help to explain some of the unexpected signaling pathways that they regulate. The importance of different subcellular localizations of $G\alpha_q$ responses is still a matter of study.

Mitochondria are essential organelles enveloped by two close but opposed membranes. The outer membrane mediates exchange between the cytosol and intermembrane space, while the inner membrane delimits the matrix space and contains respiratory complexes for oxidative phosphorylation (OXPHOS) [23]. Mitochondria can be highly dynamic organelles that fuse and divide in response to environmental stimuli, developmental status, and the energy requirements of the cell [24–26]. These events are regulated by specific proteins involved in fission and fusion, and also in the maintenance of mitochondrial distribution [27, 28]. The most notable proteins involved in mitochondrial fission/fusion processes are: the dynamin-like protein DLP1/Drp1; the small helix-rich proteins Fis1 and Mff, linked to outer mitochondrial membrane fission. The dynamin-related GTPases, mitofusins (Mfn1/2), and optic atrophy 1 (OPA1), associated with the outer and inner membrane, respectively, mediate fusion of the membranes [28–33].

The presence of signaling molecules at the mitochondria highlights the possibility of novel signaling pathways that control energy production. In the search for mitochondrial localized heterotrimeric G proteins, proteomic analysis together with fractionation and immunofluorescence analysis show that $G\alpha_q$ and $G\alpha_{11}$ target mitochondria through their N-terminal sequence. Herein, we demonstrate that $G\alpha_q$ proteins are necessary for maintenance of the proper balance between mitochondrial fusion and fission processes, and consequently for regulating the respiratory capacity of mitochondria.

Materials and Methods

Materials

pcDNA3-Gα_q and pcDNA3-Gα_q-R183C were as described elsewhere [72]. pcDNAI-Gα_q-GFP was generously provided by C. Berlot (Yale University School of Medicine, USA). Gα_q-N-terminus (1–124 aas) in pEGFP was cloned from pcDNAI-Gα_q-GFP, and Gα_q-N-terminus-FLAG in pcDNA3 was amplified by PCR. The Gα_q-N-I25/26E mutant in pEGFP was amplified by PCR using pcDNA3-Gα_q-I25/26E [72] as a template. Mt-DsRed and mt-GFP were cloned from pWPXL-mt-DsRed [73] and pWPXL-mt-GFP [73], respectively. The ER marker was obtained from Clontech (USA). pcDNA3-Gβ_1-FLAG, Gβ_2-FLAG, Gβ_4-FLAG and Gγ_2-HA were obtained from Missouri S&T cDNA Resource (USA). HA-tagged Drp1 and Drp1-K38A in pcDNA3 were kindly provided by A. van der Bliek (University of California, LA, USA). PA-mitoGFP [74] and Plasmid 23348 were purchased from Addgene (USA). The antibodies used were: Gα_q, G$\alpha_{q/11}$, Gβ and TOM20 (Santa Cruz Biotechnology); Gα_q internal, Porin-VDAC and Porin 31 HL (Calbiochem); SERCA2, Golgi [58K-9], GAPDH, Pan-cadherin, Mitofusin-1, Mitofusin-2 and LAMP1 (Abcam); Smac/diablo, Rab11, Drp1, COXI and OPA1 (BD Biosciences); Caveolin-1 (Zymed); complex II (anti-αFp70 kDa subunit) (Invitrogen); Hsp70 (BioReagents); FIS1 (BioVision); HA-tag (Roche); M2-Flag (Sigma Aldrich); complex I (anti-NDUFA9), complex III (anti-Core1) and complex V (anti-βATPase) (MitoSciences); and complex IV (anti-NDUFA4) (BioWorld Technology). Gα_q transgenic mice which over-expresses mouse Gα_q exclusively in the myocardium were a generous gift from G. W. Dorn II, Washington University at St Louis [37].

Cell culture, lysis and immunoprecipitation

NIH3T3 cells were obtained from the American Type Culture Collection (ATCC) (Manassas, VA, USA). Human embryonic kidney cells (HEK293T) were from Invitrogen (Carlsbad, CA, USA). WT, and knockout G$\alpha_{q/11}^{-/-}$ and G$\alpha_{12/13}^{-/-}$ MEFs were provided by S. Offermanns, (University of Heidelberg, Germany). WT and knockout Mfn1$^{-/-}$ and Mfn2$^{-/-}$ MEFs were a gift from D.C. Chan (Division of Biology, California Institute of Technology, UA). HeLa cells stably expressing mt-DsRed are described elsewhere [73]. All cell types were grown in Dulbecco's modified Eagle's medium (DMEM) (Sigma, St. Louis, MO, USA), supplemented with 10% fetal bovine serum (FBS) (Invitrogen, GIBCO, USA). Cells were transiently transfected either with Metafectene Pro (Biontex, USA) or Fugene 6 (Roche, Switzerland) according to the manufacturer's instructions.

Cells were washed twice with ice-cold PBS prior to lysis in 700 µl of RIPA buffer A (0.3 M NaCl, 0.1% SDS, 50 mM Tris, pH 7.4, 0.5% deoxycholate, 1 mM Na_3VO_4, 10 mM NaF, 30 mM sodium pyrophosphate, 10 mM $MgCl_2$, 1% n-dodecyl β-D-maltoside, leupeptin 5 µg/ml, aprotinin 2 µg/ml, 1 mM PMSF) for 1 h at 4°C. Extracts were cleared by centrifugation at 13,000 rpm for 15 min at 4°C and the protein concentration was determined by Bradford analysis. For OPA1 immunoprecipitation, an anti-OPA1 antibody was incubated at 4°C overnight. Protein G-sepharose was added and incubated for 1 h, and then washed several times with RIPA buffer B (buffer A with 0.01% n-dodecyl β-D-maltoside and without protease inhibitors). The samples were resuspended in Laemmli buffer. Cells were visualized with either chemiluminescence (by film acquisition or LAS3000) or infrared detection (Odyssey System). Quantifications were performed with the software indicated in the figure legends.

Imaging

For immunofluorescence, cells seeded on coverslips were washed in PBS, fixed (4% formaldehyde) and permeabilized in PBS with 0.1% Triton X-100 and 0.05% sodium deoxycholate, before staining with primary antibodies and secondary Alexa Fluor antibodies (Invitrogen, CA, USA) in blocking solution (5% goat serum). Mitochondrial morphology was determined as described elsewhere [75] and examined using a Nikon E600 microscope. Optical sections were acquired using a Leica TCS SP5 confocal system. Colocalization analyses were performed using LAS AF software (Leica Microsystems, Germany), Imaris colocalization module (Bitplane AG, Zurich, Switzerland) or ImageJ (National Institutes of Health, USA). Average mitochondrial area and length were quantified using the LAS AF software (Leica Microsystems, Germany). Scale bars of 10 μm and Z-stacks of 0.5 μm are shown (unless specified differently in the figure legends). For live imaging, cells were seeded on coverslips and transiently transfected as described above. For short-term live cell imaging, an UltraView ERS spinning disk confocal microscope (Perkin Elmer, USA) equipped with a 37°C incubation chamber with 5% CO2 was used. Z-stacks of the images were collected using a 100X NA 1.4 oil objective with a helium-neon laser at 543 nm. The Z-stacks were acquired continuously over 10 min in the spinning disk with 300 millisecond exposures. The images from the time-lapse imaging were processed using Volocity 3D image analysis software (Perkin Elmer, USA) and mounted as .MPEG4 files. For the electron microscopy, MEFs were plated in two 10 cm Ø plates for each sample and sent to the Electron Microscopy Platform (Scientific and Technological Centers, University of Barcelona, Spain) for sample preparation. Ultrathin sections (55 nm) were cut and mounted with 200 mesh cupper grid with supported film. Image acquisition was performed with a transmission electron microscope (JEOL-1010) coupled to Bioscan software (Gatan, UK).

Isolation of mitochondria

The mitochondrial isolation kit MITOISO2 (Sigma Aldrich) was utilized according to the manufacturer's instructions. The final mitochondrial pellet was layered onto a Percoll density gradient (Sigma Aldrich), and resuspended as indicated by the manufacturer.

Crude mitochondrial isolation was performed as described elsewhere [76]. For trypsin/triton digestion of crude mitochondria, 200–800 μg/ml of trypsin was added to tube T (200/+, 400/++ and 800/+++) and to tube TT, 200 μg/ml of trypsin with 2% of triton X-100 was added. All the samples were incubated at 37°C, and after 15 min, 10% FBS was added to halt digestion. The samples were centrifuged at 13,000×g for 2 min and washed twice with incubation buffer before adding the SDS-loading buffer and analyzing by Western blot. Crude mitochondria fraction from mouse heart was performed with ProteoExtract Cytosol/

Mitochondria Kit (Calbiochem), following the manufacturer's instructions. Subfractions of mouse liver mitochondria were generated as described elsewhere [41].

Cellular treatments

To label mitochondria, cells were incubated with 300 nM MitoTracker® CMXRos (Invitrogen) or were transfected with pcDNA3-mt-DsRed or pcDNA3-mt-GFP. The incubation of WT and $G\alpha_{q/11}{}^{-/-}$ MEFs with carbonyl cyanide m-chlorophenylhydrazone (CCCP) (Sigma Aldrich) (10 μM) took place in supplemented DMEM at 37°C for 6 and 3 h, respectively.

Down-regulation of murine $G\alpha_{q/11}$ proteins

shRNA-mediated knockdown of $G\alpha_{q/11}$ was performed using specific Mission shRNA and nontargeting Mission shRNA negative control (Sigma Aldrich). Lentivirus particle production was developed following the manufacturer's instructions in HEK293T cells and down-regulation was monitored by immunoblot analysis of cell lysates generated after 3 days of puromycin selection of infected cells.

Mass spectrometry analysis

Following mitochondrial Percoll gradient fractionation of NIH3T3 cells and SDS-PAGE, the gel was stained with Colloidal Coomassie Blue G250 (Sigma Aldrich) and the bands corresponding to 35 – 50 kDa were cut and sent to the PCB Proteomics Platform to proceed with mass spectrometry analysis. The related protocols can be found at http://www.pcb.ub.edu/homePCB/live/en/p1249.asp.

Mitochondrial fusion analysis

MEFs were transfected with mt-DsRed and mito-PAGFP. A cell was photobleached and photoactivated and then time lapse series of image stacks composed of 4 images (512×512) were taken every 4 s for 15 min. Intensity correlation analysis was performed against red (photobleached mt-DsRed) and green (photoactivated mito-PAGFP) using Volocity. The threshold was automatically performed [77]. The rates of fusion were analyzed using the overlap coefficient K2 (red dots containing green) and data were normalized according to the intensity of the first time point after photobleaching.

Growth Rates

Cells (5×10^4) were plated in 24-well plates in 1 ml of the indicated medium and incubated at 37°C for up to 3 days. They were counted daily using a Neubauer chamber. The culture media used were: DMEM with 5 mM of either glucose or galactose, supplemented with 10% FBS.

Cellular ATP, oxygen consumption and membrane potential

The ATP Determination Kit (Invitrogen) was used following the manufacturer's instructions. The oxygen consumption was determined in 4×10^4 intact MEFs using a Seahorse Bioscience XF96 extracellular flux analyzer following the manufacturer's instructions and using the materials provided. Protocol: 12 min of equilibration, followed by

3 measurements of 3 min, separated by mixing for 4 min. Uncoupled mitochondrial respiration was induced by injection of 1 μM CCCP. To stop the mitochondrial-dependent oxygen consumption, we utilized 1 μM Oligomycin.

To calculate the membrane potential, MEFs (5×10^6) were treated with 100 nM of the fluorescent dye TMR for 30 min at 37°C, washed with PBS and resuspended with 400 μl of trypsin. To halt trypsin digestion, 1 ml of PBS containing 5% BSA was added. The cells were passed through a flow cytometer, MoFlo (Beckman Coulter) at 590 nm.

Isolation of respiratory complexes and supercomplexes – BN-PAGE

Mitochondria were isolated from cultured cell lines as described elsewhere [78], with slight modifications [76]. Digitonin-solubilized mitochondrial proteins (50 μg) were separated on blue native gradient gels (3%-13% acrylamide).

Statistical analysis

Average mitochondrial surface area: Comparison between WT and knockout cells presented heterogeneous variance, so the Mann-Whitney non-parametric test was utilized. Comparisons between values found for shRNA presented normal distributions, which allowed the use of variance analysis, followed by Student's t-test. Mitochondrial length: Values from WT and knockout cells presented heterogeneous variance, so the Mann-Whitney non-parametric test was performed; a heterogeneous variance distribution was also found in the shRNA groups, for these values the Kruskal-Wallis test was utilized. Mitochondrial morphology: The values were analyzed by Chi-squared test, only when fewer than five values were found was the G-test employed, followed by Fisher's test. Mitochondrial fusion analysis by mt-PAGFP was performed using ANOVA. Mitochondrial membrane potential and O_2 consumption were analyzed by unpaired t-test; whereas total ATP content and Odyssey quantification of Supercomplex I+III+IV/Porin was by paired t-test. Growth rate differences were determined by one-way ANOVA followed by Tukey's Test (p-values are given in the figure legends).

Results

$G\alpha_{q/11}$ proteins localize at mitochondria

In order to search for signaling proteins located at the mitochondria, a proteomic analysis of a mitochondrial fraction, obtained from a Percoll gradient, was performed on NIH3T3 cells. Only the gel bands around the overall molecular weight of G proteins (35–56 kDa) were chosen for sample analysis. Of 56 proteins (Table S1), 49 were either mitochondrial proteins included in MitoCarta [34], or cited as putative mitochondrial-associated proteins; this validated our approach. Among them, both $G\alpha_q$ and $G\alpha_{11}$ were recognized, as were the $G\alpha_{i2-3}$ and $G\alpha_{o1}$ subunits. $G\alpha_i$ proteins had previously been reported to be located at the mitochondria [3]. MitoProt analysis of the G proteins gave the highest scores for $G\alpha_q$ and $G\alpha_{11}$ proteins: 30% and 37%, respectively (Fig. S1). Western blot analysis of the Percoll-gradient mitochondrial fraction agreed with the proteomic analysis (Fig. 1A). A band recognized by the common anti-$G\alpha_q$ and anti-$G\alpha_{11}$ antibody was present (13%) in the fraction, as was the mitochondrial protein porin (38%). In order to obtain the purest mitochondria sample, only a fraction of total porin was recovered. A crucial finding was that no plasma membrane (P-Cadherin), ER (SERCA2) or golgi contamination was present. The fraction did, however, contain lysosomes (20%) and caveolin-1 (4%), a protein that binds to $G\alpha_q$ [35] and is also present in mitochondria [36].

The subcellular localization of $G\alpha_q$ was analyzed in a transgenic mouse line containing 40 copies of the $G\alpha_q$ gene expressed in the myocardium. Mitochondria fractionation showed that approximately 10% of total $G\alpha_q$ is present in the mitochondrial fraction of the wild-type (WT) heart (Fig. 1B). Interestingly, the transgenic mice showed increased levels of $G\alpha_q$ (55% of total) in the mitochondrial fraction (Fig. 1B). Again, these data indicate the presence of $G\alpha_q$ at the mitochondria in heart tissue of wild type animals and increase amounts in the transgenic mouse line. Interestingly, these mice present dilated cardiomyopathy [37] which has been reported to be associated with increased mitochondrial ROS production [38].

On the other hand, immunofluorescence analysis of the endogenous proteins in NIH3T3 cells with anti-$G\alpha_{q/11}$ antibodies (Fig. 1C) revealed a punctuated cytoplasmic pattern coincident with the mitochondria. Expression of a functional $G\alpha_q$-GFP also showed considerable localization at the mitochondria in NIH3T3 (Fig. 1C). Taken together, these findings support the hypothesis that $G\alpha_q$ proteins are located at the mitochondria.

The N-terminal region of $G\alpha_q$ is necessary for mitochondrial targeting

Considering the possibility that $G\alpha_q$ and/or $G\alpha_{11}$ were targeted to mitochondrial membranes, we searched for putative targeting sequences. A mitochondrial target prediction by Mitoprot analysis of different G alpha subunit sequences showed that mouse $G\alpha_q$ and $G\alpha_{11}$ had 30 and 37% probability of being target to mitochondria, respectively, whereas $G\alpha_{12}$, $G\alpha_{i1-2}$ or $G\alpha_o$ had lower probabilities (Fig. S1). Chimeric proteins were designed that contained the first 124 N-terminus amino acids or the C-terminus sequence of $G\alpha_q$ fused to either GFP or Flag. The C-terminus sequence fused to GFP gave almost no detectable expression around any part of the cell. The $G\alpha_q$-protein N-terminus sequence flagged with either Flag or GFP showed mitochondrial localization (Fig. 1D), which suggests that the N-terminus of $G\alpha_q$ is sufficient for the protein to located at the the mitochondria. The $G\alpha_q$ N-terminus region contains both the S-palmitoyl cysteines (9–10 aa) required for plasma membrane binding, and also the contact sites for $G\beta\gamma$ interaction. Mutations of amino acids 25 and 26 (IE>AA) are reported to alter $G\beta\gamma$ binding and also to prevent correct palmitoylation of the $G\alpha$ subunit [39]. The N-terminus-$G\alpha_q$-IE25/26AA mutant (Fig. 1D) failed to localize at the mitochondria, suggesting that the interaction with $G\beta\gamma$ and/or the state of palmitoylation of the protein is important for mitochondrial targeting. The fact that the mutated peptide was not present at the mitochondria rules out possible artifactual localization of the chimeric protein at the mitochondria.

The $G\alpha_q\beta\gamma$ heterotrimer is localized at the outer membrane and the Ga_q subunit at the inner membrane

The previous results suggest that the $G\beta\gamma$ dimer could help to target the heterotrimer at the mitochondria. The expression of $G\beta4\gamma2$ alone or together with the $G\alpha_q$-GFP protein shows localization of both HA-tagged Gγ2 and $G\alpha_q$ with mt-DsRed (Fig. 2A and Movies S1 and S2). Similar results were obtained by expressing Gβ1γ2 together with $G\alpha_q$-GFP (Fig. S2A). The Gβγ subunits are known to localize at the ER of cells [1]. To establish whether Gβγ localization corresponded to the ER, we compared the localization of Gβ4γ2 in HeLa cells expressing mt-DsRed and ER-DsRed. Significantly more Gβ4γ2 was observed at the mitochondria than at the ER (Fig. S2B). These results confirm the localization of the heterotrimer at the mitochondria.

To examine the location of the G proteins within the mitochondrial subcompartments, we carried out trypsin digestion experiments on isolated mitochondria. Incubation of mitochondria with trypsin leads to the complete digestion of the outer membrane protein Mfn2 as well as that of the Gβ proteins (Fig. 2B), which is indicative of their outer membrane localization. The $G\alpha_{q/11}$ proteins were partially digested by trypsin, indicating that some protein was located together with Gβγ at the outer membrane facing the cytoplasm. However, a considerable amount of $G\alpha_{q/11}$ was protected from digestion, as also observed for the inner membrane protein OPA1 (see Fig. 2C for a diagram representing trypsin digestion). Sub-fractionation of mitochondrial membrane by established procedures [40, 41] yields fractions enriched in outer membrane (OM), intermembrane space (IMS), inner membrane (IM) and matrix (M). In adult mouse liver (Fig. 2D), we observed the presence of $G\alpha_{q/11}$ in the total mitochondrial fraction (TO) and associated with OM, and a relative enrichment in the IM fraction (also COXI enriched); this confirms the trypsin experimental results.

Taken together these results corroborate the presence of $G\alpha_{q/11}$ proteins in the mitochondria of different cells and tissues, and also suggest that those proteins are localized together with Gβγ at the outer membrane. A proportion of the $G\alpha_{q/11}$ subunits are protected from digestion, suggesting that they are localized inside the mitochondria.

$G\alpha_{q/11}$ deletion results in defects in mitochondrial morphology

As a first approach to determine whether $G\alpha_{q/11}$ plays a direct functional role when localized at the mitochondria, we compared mitochondria from $G\alpha_{q/11}^{-/-}$ knockout (KO) and wild type murine embryonic fibroblasts (MEFs). Confocal microscopy of cells expressing the mitochondrial target peptide mt-DsRed showed marked differences in mitochondrial distribution and shape (Fig. 3A). Notably, mitochondria from $G\alpha_{q/11}^{-/-}$ cells were compacted around the nucleus. These differences were also observed via *in vivo* time-lapse images of WT (Movie S3) and $G\alpha_{q/11}^{-/-}$ (Movie S4) MEFs. Quantification of average mitochondrial surface area (Fig. 3B) showed that in $G\alpha_{q/11}^{-/-}$ cells, the mitochondrial network is less distributed throughout the cell. Quantification of the mitochondrial length showed that the $G\alpha_{q/11}^{-/-}$ mitochondria were also more fragmented than in WT cells (Fig. 3C). These results were corroborated using WT MEFs treated with shRNA against $G\alpha_q$ (Fig. S3A). The $G\alpha_q$-down-regulated cells showed an increased compaction of their mitochondrial network and more fragmented mitochondria (Fig. 3D–F) relative to the scrambled shRNA. When $G\alpha_q$ and $G\alpha_q$-GFP (Fig. S3B) were re-expressed in the $G\alpha_{q/11}^{-/-}$ MEF cells, both proteins restored the normal mitochondrial morphology and resulted in a fused mitochondrial network. The $G\alpha_q$ N-terminus (the first 124 aas) did not achieve this

(Fig. S3B), demonstrating that the whole protein is required for recovery of the mitochondrial phenotype.

To corroborate the immunofluorescence results, the ultrastructure of the $G\alpha_{q/11}{}^{-/-}$ mitochondria was examined by transmission electron microscopy (TEM). The TEM images revealed mitochondrial abnormalities (Fig. 3G, 4–9) compared with WT (Figure 3G1 and 3G2) or $G\alpha_{12/13}{}^{-/-}$ mitochondria (Fig. 3G3 and S3C). The $G\alpha_{q/11}{}^{-/-}$ mitochondria showed localized swelling accompanied by a constriction along the length of the mitochondria (Fig. 3G4 and 3G5). Almost no elongated mitochondria were found, thereby corroborating the immunofluorescence results. Remarkably, some mitochondria seem to be devoid of a cristae structure (Fig. 3G5–7) and the openings of cristae junctions appeared very narrow (Fig. 3G8). We also observed an increased number of autophagosomes containing mitochondrial remnants (Fig. 3G9), suggesting a greater turnover of damaged mitochondria through the process called mitophagy. Overall, these results suggest that $G\alpha_{q/11}$ proteins play an essential role in mitochondrial morphology

$G\alpha_q$-GDP state is needed to coordinate elongation of the mitochondrial network

The aforementioned changes in mitochondrial morphology associated with alterations in $G\alpha_q$ expression could be the result of alterations in the processes of fission or fusion. To determine whether $G\alpha_{q/11}$ are involved in mitochondrial fusion, we transfected a photoactivated mito-PAGFP into WT (Movie S5) and $G\alpha_{q/11}{}^{-/-}$ (Movie S6) MEFs. A constant increase in mitochondrial fusion events over time was detected in both cell types, but the rate of mitochondrial fusion in the $G\alpha_{q/11}{}^{-/-}$ cells was significantly lower than that in WT MEFs (Fig. 4A). These results suggest that a lack of $G\alpha_{q/11}$ affects mitochondria fusion events over time.

To study the effect of $G\alpha_q$ on fusion events further, we expressed $G\alpha_q$ in $Mfn2^{-/-}$ and $Mfn1^{-/-}$ depleted MEFs. It is well documented that Mfn1 and Mfn2 are involved in mitochondrial fusion and, in their absence, mitochondria present a fragmented phenotype (Fig. 4B) [42]. $G\alpha_q$ expression in these cells induced a significant increase in the elongation of the $Mfn2^{-/-}$ mitochondria (Fig. 4C), which indicates that $G\alpha_q$ expression promotes fusion. As expected, $G\alpha_q$ was unable to induce elongation in $Mfn1^{-/-}$ cells, since the protein is essential for mitochondrial fusion, which corroborates previous findings [42]. The activated form of $G\alpha_q$, $G\alpha_q$-R183C, did not produce the same effect (Fig. S4A). These results suggest that a GDP state of $G\alpha_q$ is needed for this function.

In contrast, expression of $G\beta2\gamma2$ in $Mfn2^{-/-}$ cells promoted mitochondrial bundle-like aggregation and perinuclear clustering (Fig. 4D) similar to those seen following mitofusin overexpression [43]. However, when $G\alpha_q$ was expressed alone or together with the heterodimer, a hyperfused-mitochondrial network was observed in both WT and $Mfn2^{-/-}$ cells (Fig. 4D). The fact that $G\beta\gamma$ did not phenocopy the effect of $G\alpha_q$ suggests that these subunits play complementary roles at the mitochondria; this provides further evidence that $G\alpha_{q/11}$ regulates fusion and/or fission events at the mitochondria.

Gα_q stabilizes mitochondrial fusion, blocking fragmentation induced by Drp1 expression

Expression in cells of the dynamin-like protein, Drp1, induces strong mitochondria fragmentation (fission) in contrast to the expression of its mutant form Drp1K38A (Fig. 5A and S5). We used the fragmentation capacity of Drp1 as another approach to study the effect of Gα_q on mitochondrial fission. The fragmentation induced by Drp1 was significantly diminished upon Gα_q expression in WT cells (Fig. 5B and 5C). Mitochondria elongation was also augmented in G$\alpha_{q/11}{}^{-/-}$ cells expressing Drp1K38A, which recovered the fragmented phenotype (Fig. S5). Gα_q acts as a potent inhibitor of mitochondrial fission, with its action depending on Drp1 at the mitochondria.

MEFs were treated with the uncoupling agent CCCP, which reduces mitochondrial fusion through dissipation of the mitochondrial membrane potential (ΔΨm) and OPA1 degradation. The fragmentation of mitochondria observed in the presence of CCCP (10 μM) decreased significantly in the presence of Gα_q (Fig. 5A, C and S5). Analysis of the OPA1 isoforms shows that CCCP could induce the degradation of OPA1, decreasing the higher isoforms (bands a and b) and increasing bands d and e (Fig. 5D), as expected. Consistently with this, cells expressing Gα_q present less decrease in bands b and e upon CCCP treatment. A change in the proportion of OPA1 bands was also observed in the untreated Gα_q and Gα_{11} knock-out cells (Fig. 5E), which presented higher levels of bands b and e. We detected no major changes in the expression of the fusion and fission proteins (Fig. S5B) that could explain these effects. The results suggest that Gα_q and Gα_{11} affect the proteolytic cleavage of OPA1 protein via either a direct or indirect effect, thus impinging on the mitochondria fission and cristae structure.

A lack of G$\alpha_{q/11}$ proteins leads to significant decreases in ΔΨm, overall respiratory capacity, ATP production and OXPHOS dependent growth

The results suggest that Gα_q and Gα_{11} proteins are necessary to maintain a proper balance of fusion and fission, and also for maintaining crest morphology. At the inner mitochondrial membrane, a proton gradient that drives ATP production is created by the respiratory complexes passing electrons through the electron transport chain and giving rise to the ΔΨm. To establish whether G$\alpha_{q/11}$ proteins are necessary for normal mitochondrial bioenergetics, we first measured the intensity of tetramethyl rhodamine (TMR) fluorescence. We determined that the ΔΨm of G$\alpha_{q/11}{}^{-/-}$ cells was significantly lower than that of WT cells (Fig. 6A). A recovery of the G$\alpha_{q/11}{}^{-/-}$ cells through expression of Gα_q prevented this decrease in ΔΨm. In addition, we determined the endogenous ATP levels and the O_2 consumption rates (OCRs) in WT and G$\alpha_{q/11}{}^{-/-}$ cells (Fig. 6B and 6C). Cells lacking G$\alpha_{q/11}$ have 15% less cellular ATP (Fig. 6B) and lower OCRs both under baseline conditions and when maximum respiratory capacity is activated by mitochondrial depolarization with CCCP (Fig. 6C).

To gain a fuller understanding of the underlying nature of the mitochondrial electron transport chain alterations, we determined how the absence of G$\alpha_{q/11}$ alters the assembly of the respiratory complexes using BN-PAGE followed by immunoblotting for subunits of the respiratory chain (Fig. 6D–H). G$\alpha_{q/11}{}^{-/-}$ cells had reduced amounts of dimer complex V (Fig. 6D). Moreover, significantly less of the supercomplexes I+III+IV (Fig. 6I) was observed. The critical reduction in larger complexes could be related to the narrow and disrupted cristae observed by TEM (Fig. 3G). Therefore, the absence of $G\alpha_{q/11}$ results in assembly disorganization of the respiratory supercomplexes which alters organelle energy production.

To determine whether the observed alterations in mitochondrial OXPHOS promoted by a lack of $G\alpha_{q/11}$ were functionally relevant, we studied the growth of the cells in a medium in which glucose was substituted by galactose; conditions that render the cells highly dependent on ATP produced by OXPHOS. Thus, the doubling time (DT) of both WT and $G\alpha_{q/11}{}^{-/-}$ cells increases in galactose compared to that in glucose as a consequence of the adaptation to a more OXPHOS demanding medium (Fig. 6J). The increase in DT is higher in KO cells than in controls (1.44 vs. 1.25), which shows that $G\alpha_{q/11}{}^{-/-}$ cells have more difficulties adapting to galactose. Altogether, these results demonstrate that $G\alpha_{q/11}$ cells are required not only for proper mitochondrial dynamics but also for OXPHOS function.

Discussion

Our studies provide insight into the mitochondrial location and functions of the G proteins, focusing on the $G\alpha_q$ family of proteins, which are distinct from their capacity to signal through GPCRs at the plasma membrane. The results establish a previously unknown link between mitochondrial fission and fusion, energy metabolism and the $G\alpha_q$ class of G proteins. The heterotrimeric G protein ($G\alpha_{q/11}\beta\gamma$) in its basal state (GDP form) is found at the outer mitochondrial membrane; whereas the alpha subunit ($G\alpha_{q/11}$) is alone inside the organelle. At the outer mitochondrial membrane, $G\alpha_q\beta\gamma$ induces mitochondrial elongation dependent on the activity of mitofusin-1 and also reduces Drp1 induction of fission. The absence of $G\alpha_{q/11}$ affects OPA-1 isoforms, cristae structure, membrane potential and organelle bioenergetics, accompanied by a reduction in respiratory supercomplex assembly. The presence of $G\alpha_{q/11}$ proteins at the mitochondria serves as a new non-canonical pathway that stabilizes elongated mitochondria and regulates energy production, thereby linking organelle dynamics and physiology.

The role and location of G proteins at the mitochondria has not previously been explored in detail, despite the presence of these proteins in other endomembranes [44–49]. Nevertheless, there are recent reports of $G\alpha_i$, $G\alpha_{12}$ and $G\beta_2$ localization at mitochondria [2–4]. Adding to what has already been reported, $G\alpha_{o1}$, $G\alpha_{11}$, $G\alpha_{i2-3}$, $G\beta_1$, $G\beta_4$ and $G\gamma 2$ were found to be localized at the mitochondria in the work reported here. Thus, taken together, this amounts to strong support for the mitochondrial localization of heterotrimeric G proteins. Although the mitochondrial targeting signal of the Gα subunits is located in the N-terminus (124 aa) and this is sufficient to confer mitochondrial location, we show that the binding to Gβγ [50] provide further support for this targeting. Taking into account that WD-propeller proteins cannot cross through the TOM complex [51] and that we and others [4] found Gβγ located at the outer membrane, it seems that only the Gα subunits can cross this membrane. At least for $G\alpha_q$, its dual location may be necessary for the coordination of the fusion of both the outer and the inner mitochondrial membrane. Both $G\alpha_{12}$ [2] and $G\alpha_q$ bind to the chaperon protein Hsp90 (unpublished results) and it is known that $G\alpha_{12}$ requires Hsp90 for mitochondrial targeting [2]. It is most likely that chaperone proteins are involved in the unfolding process necessary for crossing through the TOM complex [52]. So far we have not detected any proteolytic cleavage of Gα_q. So, the mechanism of entry of the Gα subunits is still unclear and will require further research.

The mechanism of activation and the effectors downstream from the mitochondrial-located G proteins are still unknown. However, recent reports localized two different GPCRs at this organelle: the CB_1 receptor, found at the outer mitochondria membrane of neurons [53]; and a functional angiotensin system at the inner membrane [54]. Those authors demonstrate that Ang II type 1 and 2 receptors are present in this subcompartment of the mitochondria and that the activation of the mitochondrial angiotensin system is coupled to nitric oxide production which alters the respiratory capacity. These findings raise the possibility that GPCRs located at the mitochondria could couple to the G proteins also located at this organelle. The presence at the mitochondria of G protein-effectors or binding partners such as MAPKs, Akt, GRK2 and PKC [5, 6] also supports the signaling of G proteins at mitochondria. However, the fact that the Gβ_2 subunit [4] binds directly to an intrinsic mitochondrial protein such as mitofusin 1, raises the possibility that mitochondrial proteins may act as receptor/effectors for a a new non-canonical G protein effect.

G$\alpha_{q/11}$-depleted cells presented mitochondrial fragmentation and alterations in cristae; conversely, increases in Gα_q levels elongate mitochondria. These alterations are reminiscent of those found in cells depleted in Mfns1–2 [42] and OPA1 [55]. Meanwhile, expression of Mfns1–2 or Gβγ leads to the formation of clusters of mitochondria due to outer membrane fusion [4, 56], but these clusters are not present when Gα_q is co-expressed. We propose a mechanism in which Gα_q and Gβγ are necessary for mitochondria fusion via the coordinated regulation of the Mfn1 protein. However, mitochondria elongation can also be the result of inhibition of fission. It is particularly interesting that Gα_q expression reduces Drp1 function. The Drp1 protein is recruited from the cytoplasm to the outer mitochondrial membrane where it forms assemblies and tubule constrictions around the organelle and, consequently, produces fission. Drp1 is posttranslationally modified by a variety of enzymes (phosphorylation, sumoylation, ubiquitination, S-nitrosylation), which highlights its complex regulation [57]. Our findings demonstrate that Gα_q regulate mitochondrial morphology and respiratory efficiency through a Mfn1 and Drp1-dependent mechanisms.

Mitochondria fusion involves the coordination of both the outer and inner membrane [33, 57]. Our results suggest that G$\alpha_{q/11}$ can also impinge on the inner membrane and crest morphology. G$\alpha_{q/11}$ effects could be explained by the altered processing of OPA1. Post-transcriptional regulation of OPA1 is rather complex, added to constitutive processing by different proteases (i-AAA, m-AAA and Parl) [58], which generate long and short OPA1 isoforms, all of which are required for mitochondrial fusion. L- and S-forms of OPA1 (a-b and c-d-e, respectively) form oligomers and keep cristae junctions tightly closed, thereby preventing cytosolic release of cytochrome *c* [59]. Under conditions of mitochondrial membrane depolarization (or CCCP treatment), ATP deficiency or apoptosis, the L-OPA1 isoforms undergo inducible cleavage by OMA1 which generates S-OPA1 forms (d and e), resulting in mitochondria fragmentation. It is interesting to note that G$\alpha_{q/11}$-depleted cells that have reduced ATP due to lower membrane potential and fragmentation, show an increase in L-forms (band b) and also in S-forms (band e). The increase in band e could be related to the lower membrane potential and is in agreement with the fact that mitochondria are fragmented. The higher band b, however, can only be a consequence of $G\alpha_{q/11}$ altering OPA1 processing. We consider that the mechanism of action of $G\alpha_{q/11}$ does not directly inhibit OMA1 function, since $G\alpha_{q/11}$-depleted cells present an increase in band e. Therefore, we propose that $G\alpha_{q/11}$ affects the processing of OPA1 isoforms by altering membrane potential and inner membrane fusion processes.

Our data also indicate that $G\alpha_{q/11}$ are required to maintain the proper organization of the respiratory complexes. Elongated mitochondria have higher levels of the dimeric form of ATPase, associated with increased efficiency in ATP production [60]. The absence of $G\alpha_{q/11}$ reduces not only this dimeric form (CV) but it also provokes an important reduction in supercomplexes containing complex I [61, 62]. A primary consequence of the alteration in mitochondrial elongation and cristae organization by the absence of $G\alpha_{q/11}$, was a decrease in energy transfer. These results confirm previous findings linking mitochondrial morphology and energy fluxes [63]. OPA1 regulates cristae shape, organization and dynamics [59, 64] and has been shown to interact directly with OXPHOS complexes I, II and III but not IV [65]. More recently, the lack of OPA1 or its processing by specific proteases that induces cristae remodeling was shown to consequently reduce the amount of both respiratory supercomplexes containing complex I and complex I-dependent respiration [66].

Under normal conditions, mitochondrial fusion and fission take place at a balanced rate and thus a relatively constant tubular morphology is maintained. However, perturbation of the fission/fusion balance has been found to be associated with numerous human diseases [33, 67]. Our findings raise the possibility that the non-canonical mitochondrial-function of $G\alpha_q$ may also account for some of the known functions of $G\alpha_q$ otherwise attributed to other pathways. Particularly interesting is the fact that $G\alpha_q$ signaling is essential for cardiomyocyte hypertrophy and proliferation during development [68]. However, it is also linked to hypertrophy of the adult myocardium and subsequent heart failure [69] where mitochondria need to sustain a high-energy demand [70] to avoid cell death under pathological conditions [71]. Therefore, understanding the functional role of $G\alpha_q$ at the mitochondria may open up new approaches to therapeutic treatments for cardiac diseases as well as other diseases.

Supplementary Material

Refer to Web version on PubMed Central for supplementary material.

Acknowledgments

We thank M. Pons, H. Rebollo and E. Spriet (MIC, Bergen, Norway) for assistance with live-cell imaging, and S. Sollecito for technical help. This work was supported by grants from the Spanish *Ministerio de Economia y Competitividad* (BFU2011-30080, SAF2009-08007 & CSD2007-00020), and the *Comunidad de Madrid* regional authorities (S2011/BMD-2402). C. B. was supported by a JAE-Pre fellowship (CSIC).

References

1. Hewavitharana T, Wedegaertner PB. Non-canonical signaling and localizations of heterotrimeric G proteins. Cell Signal. 2011

2. Andreeva AV, Kutuzov MA, Voyno-Yasenetskaya TA. G alpha12 is targeted to the mitochondria and affects mitochondrial morphology and motility. FASEB J. 2008; 22:2821–2831. [PubMed: 18367648]

3. Lyssand JS, Bajjalieh SM. The heterotrimeric [corrected] G protein subunit G alpha i is present on mitochondria. FEBS Lett. 2007; 581:5765–5768. [PubMed: 18037379]

4. Zhang J, et al. G-protein beta2 subunit interacts with mitofusin 1 to regulate mitochondrial fusion. Nat Commun. 2010; 1:101. [PubMed: 20981029]

5. Antico Arciuch VG, Alippe Y, Carreras MC, Poderoso JJ. Mitochondrial kinases in cell signaling: Facts and perspectives. Adv Drug Deliv Rev. 2009; 61:1234–1249. [PubMed: 19733603]

6. Fusco A, et al. Mitochondrial localization unveils a novel role for GRK2 in organelle biogenesis. Cell Signal. 2011

7. Hepler JR, Gilman AG. G proteins. Trends Biochem Sci. 1992; 17:383–387. [PubMed: 1455506]

8. Mizuno N, Itoh H. Functions and regulatory mechanisms of Gq-signaling pathways. Neurosignals. 2009; 17:42–54. [PubMed: 19212139]

9. Sengupta P, Philip F, Scarlata S. Caveolin-1 alters Ca(2+) signal duration through specific interaction with the G alpha q family of G proteins. J Cell Sci. 2008; 121:1363–1372. [PubMed: 18397999]

10. Rochdi MD, et al. Regulation of GTP-binding protein alpha q (Galpha q) signaling by the ezrin-radixin-moesin-binding phosphoprotein-50 (EBP50). J Biol Chem. 2002; 277:40751–40759. [PubMed: 12193606]

11. Little KD, Hemler ME, Stipp CS. Dynamic regulation of a GPCR-tetraspanin-G protein complex on intact cells: central role of CD81 in facilitating GPR56-Galpha q/11 association. Mol Biol Cell. 2004; 15:2375–2387. [PubMed: 15004227]

12. Sugawara Y, et al. The lipid raft proteins flotillins/reggies interact with Galphaq and are involved in Gq-mediated p38 mitogen-activated protein kinase activation through tyrosine kinase. Cell Signal. 2007; 19:1301–1308. [PubMed: 17307333]

13. Boulay G, et al. Cloning and expression of a novel mammalian homolog of Drosophila transient receptor potential (Trp) involved in calcium entry secondary to activation of receptors coupled by the Gq class of G protein. J Biol Chem. 1997; 272:29672–29680. [PubMed: 9368034]

14. Sjogren B, Neubig RR. Thinking outside of the "RGS box": new approaches to therapeutic targeting of regulators of G protein signaling. Mol Pharmacol. 2010; 78:550–557. [PubMed: 20664002]

15. Hepler JR, Berman DM, Gilman AG, Kozasa T. RGS4 and GAIP are GTPase-activating proteins for Gq alpha and block activation of phospholipase C beta by gamma-thio-GTP-Gq alpha. Proc Natl Acad Sci U S A. 1997; 94:428–432. [PubMed: 9012799]

16. Carman CV, et al. Selective regulation of Galpha(q/11) by an RGS domain in the G protein-coupled receptor kinase, GRK2. J Biol Chem. 1999; 274:34483–34492. [PubMed: 10567430]

17. Usui H, et al. RGS domain in the amino-terminus of G protein-coupled receptor kinase 2 inhibits Gq-mediated signaling. Int J Mol Med. 2000; 5:335–340. [PubMed: 10719047]

18. Momotani K, et al. p63RhoGEF Couples G{alpha}q/11-Mediated Signaling to Ca2+ Sensitization of Vascular Smooth Muscle Contractility. Circ Res. 2011; 109:993–1002. [PubMed: 21885830]

19. Bence K, Ma W, Kozasa T, Huang XY. Direct stimulation of Bruton's tyrosine kinase by G(q)-protein alpha-subunit. Nature. 1997; 389:296–299. [PubMed: 9305846]

20. Garcia-Hoz C, et al. G alpha(q) acts as an adaptor protein in protein kinase C zeta (PKCzeta)-mediated ERK5 activation by G protein-coupled receptors (GPCR). J Biol Chem. 2010; 285:13480–13489. [PubMed: 20200162]

21. Tall GG, Krumins AM, Gilman AG. Mammalian Ric-8A (synembryn) is a heterotrimeric Galpha protein guanine nucleotide exchange factor. J Biol Chem. 2003; 278:8356–8362. [PubMed: 12509430]

22. Popova JS, Garrison JC, Rhee SG, Rasenick MM. Tubulin, Gq, and phosphatidylinositol 4,5-bisphosphate interact to regulate phospholipase Cbeta1 signaling. J Biol Chem. 1997; 272:6760–6765. [PubMed: 9045709]

23. Frey TG, Mannella CA. The internal structure of mitochondria. Trends Biochem Sci. 2000; 25:319–324. [PubMed: 10871882]

24. Chan D, Frank S, Rojo M. Mitochondrial dynamics in cell life and death. Cell Death Differ. 2006; 13:680–684. [PubMed: 16410792]
25. Frazier AE, Kiu C, Stojanovski D, Hoogenraad NJ, Ryan MT. Mitochondrial morphology and distribution in mammalian cells. Biol Chem. 2006; 387:1551–1558. [PubMed: 17132100]
26. Campello S, Scorrano L. Mitochondrial shape changes: orchestrating cell pathophysiology. EMBO Rep. 2010; 11:678–684. [PubMed: 20725092]
27. Liesa M, Palacin M, Zorzano A. Mitochondrial dynamics in mammalian health and disease. Physiol Rev. 2009; 89:799–845. [PubMed: 19584314]
28. Westermann B. Mitochondrial fusion and fission in cell life and death. Nat Rev Mol Cell Biol. 2010; 11:872–884. [PubMed: 21102612]
29. Koshiba T, et al. Structural basis of mitochondrial tethering by mitofusin complexes. Science. 2004; 305:858–862. [PubMed: 15297672]
30. Ishihara N, Fujita Y, Oka T, Mihara K. Regulation of mitochondrial morphology through proteolytic cleavage of OPA1. EMBO J. 2006; 25:2966–2977. [PubMed: 16778770]
31. Cipolat S, Martins de Brito O, Dal Zilio B, Scorrano L. OPA1 requires mitofusin 1 to promote mitochondrial fusion. Proc Natl Acad Sci U S A. 2004; 101:15927–15932. [PubMed: 15509649]
32. Malka F, et al. Separate fusion of outer and inner mitochondrial membranes. EMBO Rep. 2005; 6:853–859. [PubMed: 16113651]
33. Chen H, Chan DC. Emerging functions of mammalian mitochondrial fusion and fission. Hum Mol Genet. 2005; 14(Spec No. 2):R283–R289. [PubMed: 16244327]
34. Pagliarini DJ, et al. A mitochondrial protein compendium elucidates complex I disease biology. Cell. 2008; 134:112–123. [PubMed: 18614015]
35. Bhatnagar A, Sheffler DJ, Kroeze WK, Compton-Toth B, Roth BL. Caveolin-1 interacts with 5-HT2A serotonin receptors and profoundly modulates the signaling of selected Galphaq-coupled protein receptors. J Biol Chem. 2004; 279:34614–34623. [PubMed: 15190056]
36. Li WP, Liu P, Pilcher BK, Anderson RG. Cell-specific targeting of caveolin-1 to caveolae, secretory vesicles, cytoplasm or mitochondria. J Cell Sci. 2001; 114:1397–1408. [PubMed: 11257005]
37. D'Angelo DD, et al. Transgenic Galphaq overexpression induces cardiac contractile failure in mice. Proc Natl Acad Sci U S A. 1997; 94:8121–8126. [PubMed: 9223325]
38. Dai DF, et al. Mitochondrial oxidative stress mediates angiotensin II-induced cardiac hypertrophy and Galphaq overexpression-induced heart failure. Circ Res. 2011; 108:837–846. [PubMed: 21311045]
39. Evanko DS, Thiyagarajan MM, Wedegaertner PB. Interaction with Gbetagamma is required for membrane targeting and palmitoylation of Galpha(s) and Galpha(q). J Biol Chem. 2000; 275:1327–1336. [PubMed: 10625681]
40. Cipolat S, et al. Mitochondrial rhomboid PARL regulates cytochrome c release during apoptosis via OPA1-dependent cristae remodeling. Cell. 2006; 126:163–175. [PubMed: 16839884]
41. Darshi M, et al. ChChd3, an inner mitochondrial membrane protein, is essential for maintaining crista integrity and mitochondrial function. J Biol Chem. 2011; 286:2918–2932. [PubMed: 21081504]
42. Chen H, et al. Mitofusins Mfn1 and Mfn2 coordinately regulate mitochondrial fusion and are essential for embryonic development. J Cell Biol. 2003; 160:189–200. [PubMed: 12527753]
43. Santel A, Fuller MT. Control of mitochondrial morphology by a human mitofusin. J Cell Sci. 2001; 114:867–874. [PubMed: 11181170]
44. Ercolani L, et al. Membrane localization of the pertussis toxin-sensitive G-protein subunits alpha i-2 and alpha i-3 and expression of a metallothionein-alpha i-2 fusion gene in LLC-PK1 cells. Proc Natl Acad Sci U S A. 1990; 87:4635–4639. [PubMed: 1693774]
45. Leyte A, Barr FA, Kehlenbach RH, Huttner WB. Multiple trimeric G-proteins on the trans-Golgi network exert stimulatory and inhibitory effects on secretory vesicle formation. EMBO J. 1992; 11:4795–4804. [PubMed: 1464309]
46. Pimplikar SW, Simons K. Regulation of apical transport in epithelial cells by a Gs class of heterotrimeric G protein. Nature. 1993; 362:456–458. [PubMed: 8385268]

47. Stow JL, Heimann K. Vesicle budding on Golgi membranes: regulation by G proteins and myosin motors. Biochim Biophys Acta. 1998; 1404:161–171. [PubMed: 9714787]

48. Sato M, Blumer JB, Simon V, Lanier SM. Accessory proteins for G proteins: partners in signaling. Annu Rev Pharmacol Toxicol. 2006; 46:151–187. [PubMed: 16402902]

49. Chisari M, Saini DK, Kalyanaraman V, Gautam N. Shuttling of G protein subunits between the plasma membrane and intracellular membranes. J Biol Chem. 2007; 282:24092–24098. [PubMed: 17576765]

50. Resh MD. Palmitoylation of ligands, receptors, and intracellular signaling molecules. Sci STKE. 2006; 2006:re14. [PubMed: 17077383]

51. Dagda RK, Barwacz CA, Cribbs JT, Strack S. Unfolding-resistant translocase targeting: a novel mechanism for outer mitochondrial membrane localization exemplified by the Bbeta2 regulatory subunit of protein phosphatase 2A. J Biol Chem. 2005; 280:27375–27382. [PubMed: 15923182]

52. Chacinska A, Koehler CM, Milenkovic D, Lithgow T, Pfanner N. Importing mitochondrial proteins: machineries and mechanisms. Cell. 2009; 138:628–644. [PubMed: 19703392]

53. Benard G, et al. Mitochondrial CB(1) receptors regulate neuronal energy metabolism. Nat Neurosci. 2012; 15:558–564. [PubMed: 22388959]

54. Abadir PM, et al. Identification and characterization of a functional mitochondrial angiotensin system. Proc Natl Acad Sci U S A. 2011; 108:14849–14854. [PubMed: 21852574]

55. Griparic L, van der Wel NN, Orozco IJ, Peters PJ, van der Bliek AM. Loss of the intermembrane space protein Mgm1/OPA1 induces swelling and localized constrictions along the lengths of mitochondria. J Biol Chem. 2004; 279:18792–18798. [PubMed: 14970223]

56. Santel A, et al. Mitofusin-1 protein is a generally expressed mediator of mitochondrial fusion in mammalian cells. J Cell Sci. 2003; 116:2763–2774. [PubMed: 12759376]

57. Otera H, Mihara K. Molecular mechanisms and physiologic functions of mitochondrial dynamics. J Biochem. 2011; 149:241–251. [PubMed: 21233142]

58. Scorrano L. Keeping mitochondria in shape: a matter of life and death. Eur J Clin Invest. 2013; 43:886–893. [PubMed: 23869410]

59. Frezza C, et al. OPA1 controls apoptotic cristae remodeling independently from mitochondrial fusion. Cell. 2006; 126:177–189. [PubMed: 16839885]

60. Strauss M, Hofhaus G, Schroder RR, Kuhlbrandt W. Dimer ribbons of ATP synthase shape the inner mitochondrial membrane. EMBO J. 2008; 27:1154–1160. [PubMed: 18323778]

61. Acin-Perez R, et al. Respiratory complex III is required to maintain complex I in mammalian mitochondria. Mol Cell. 2004; 13:805–815. [PubMed: 15053874]

62. Acin-Perez R, Fernandez-Silva P, Peleato ML, Perez-Martos A, Enriquez JA. Respiratory active mitochondrial supercomplexes. Mol Cell. 2008; 32:529–539. [PubMed: 19026783]

63. Piquereau J, et al. Down-regulation of OPA1 alters mouse mitochondrial morphology, PTP function, and cardiac adaptation to pressure overload. Cardiovasc Res. 2012; 94:408–417. [PubMed: 22406748]

64. Meeusen S, et al. Mitochondrial inner-membrane fusion and crista maintenance requires the dynamin-related GTPase Mgm1. Cell. 2006; 127:383–395. [PubMed: 17055438]

65. Zanna C, et al. OPA1 mutations associated with dominant optic atrophy impair oxidative phosphorylation and mitochondrial fusion. Brain. 2008; 131:352–367. [PubMed: 18222991]

66. Cogliati S, et al. Mitochondrial cristae shape determines respiratory chain supercomplexes assembly and respiratory efficiency. Cell. 2013; 155:160–171. [PubMed: 24055366]

67. Bossy-Wetzel E, Barsoum MJ, Godzik A, Schwarzenbacher R, Lipton SA. Mitochondrial fission in apoptosis, neurodegeneration and aging. Curr Opin Cell Biol. 2003; 15:706–716. [PubMed: 14644195]

68. Offermanns S, et al. Embryonic cardiomyocyte hypoplasia and craniofacial defects in G alpha q/G alpha 11-mutant mice. EMBO J. 1998; 17:4304–4312. [PubMed: 9687499]

69. Adams JW, Brown JH. G-proteins in growth and apoptosis: lessons from the heart. Oncogene. 2001; 20:1626–1634. [PubMed: 11313910]

70. Miyamoto S, Murphy AN, Brown JH. Akt mediated mitochondrial protection in the heart: metabolic and survival pathways to the rescue. J Bioenerg Biomembr. 2009; 41:169–180. [PubMed: 19377835]

71. Zak R, Rabinowitz M, Rajamanickam C, Merten S, Kwiatkowska-Patzer B. Mitochondrial proliferation in cardiac hypertrophy. Basic Res Cardiol. 1980; 75:171–178. [PubMed: 6446287]

72. Johansson BB, Minsaas L, Aragay AM. Proteasome involvement in the degradation of the G(q) family of Galpha subunits. FEBS J. 2005; 272:5365–5377. [PubMed: 16218966]

73. Liesa M, et al. Mitochondrial fusion is increased by the nuclear coactivator PGC-1beta. PLoS One. 2008; 3:e3613. [PubMed: 18974884]

74. Karbowski M, et al. Quantitation of mitochondrial dynamics by photolabeling of individual organelles shows that mitochondrial fusion is blocked during the Bax activation phase of apoptosis. J Cell Biol. 2004; 164:493–499. [PubMed: 14769861]

75. Merkwirth C, et al. Prohibitins control cell proliferation and apoptosis by regulating OPA1-dependent cristae morphogenesis in mitochondria. Genes Dev. 2008; 22:476–488. [PubMed: 18281461]

76. Acin-Perez R, et al. Cyclic AMP produced inside mitochondria regulates oxidative phosphorylation. Cell Metab. 2009; 9:265–276. [PubMed: 19254571]

77. Costes SV, et al. Automatic and quantitative measurement of protein-protein colocalization in live cells. Biophys J. 2004; 86:3993–4003. [PubMed: 15189895]

78. Schagger H. Native electrophoresis for isolation of mitochondrial oxidative phosphorylation protein complexes. Methods Enzymol. 1995; 260:190–202. [PubMed: 8592444]

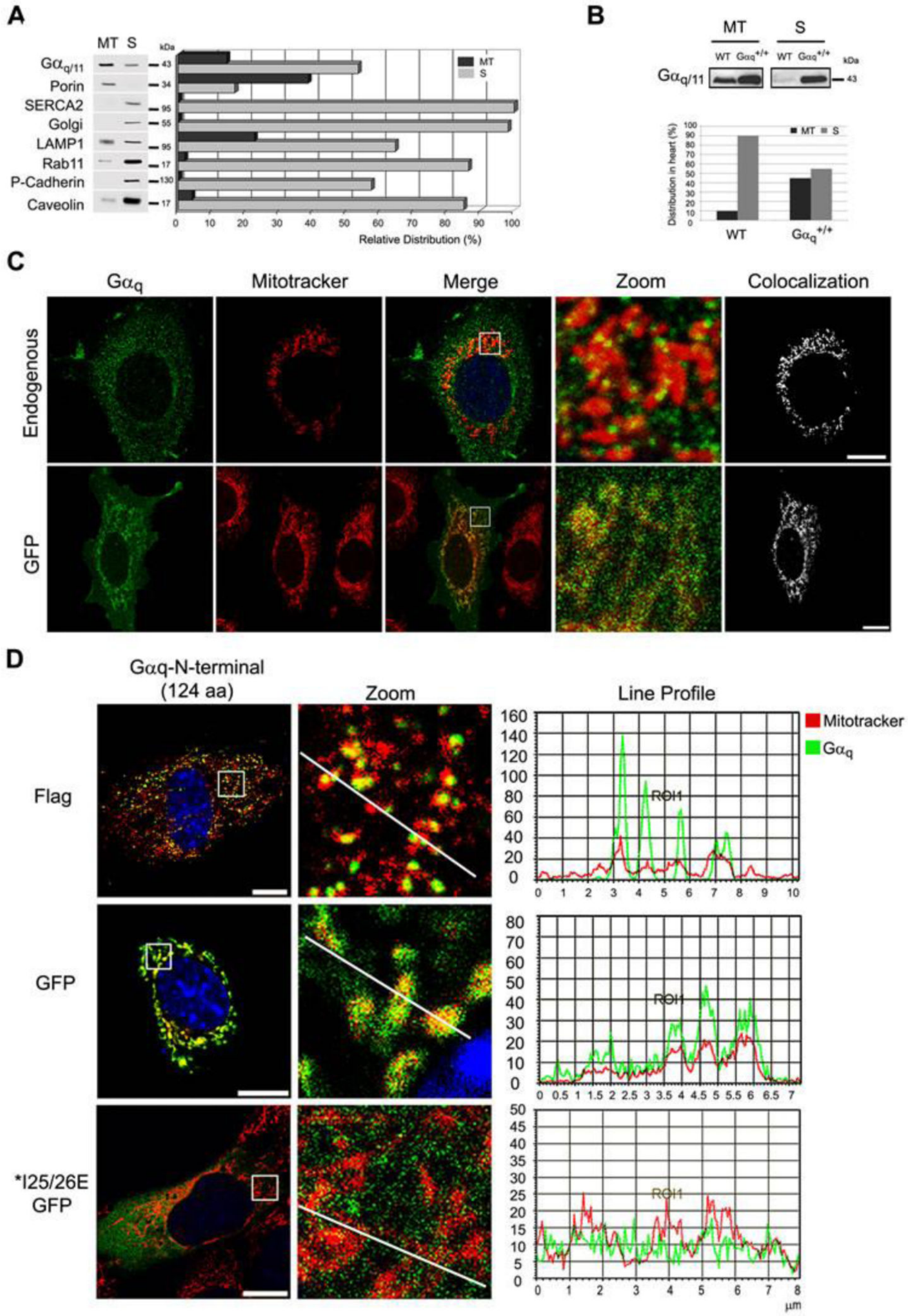

Fig. 1. Gα_q and Gα_{11} are localized at the mitochondria

(A) Distribution of endogenous G$\alpha_{q/11}$ and organelle markers in the mitochondrial (MT) and supernatant (S) fractions obtained by Percoll gradient of NIH3T3 cells. The MT fraction was resuspended in 1/5 of initial volume, and equal volumes of MT and S fractions were loaded in the gel and immunoblotted with: anti-G$\alpha_{q/11}$, Porin (mitochondria), SERCA2 (ER), Golgi, LAMP1 (lysosomes), Rab11 (ribosomes), P-cadherin (PM) and Caveolin-1 as a protein that binds to Gα_q [35] and is present at the mitochondria [36]. Quantification was performed by Multi-Gauge. **(B)** Gα_q heart-specific transgenic mouse (G$\alpha_q^{+/+}$) show increased amount of Gα_q at the mitochondria. The mitochondrial (MT) and supernatant fraction (S) were immunoblotted with G$\alpha_{q/11}$ antibody. Quantification was performed by Alpha Ease FC. **(C)** Confocal micrographs of NIH3T3 cells (endogenous) immunostained with anti-G$\alpha_{q/11}$ or expressing Gα_q-GFP. Colocalization was performed by LAS AF. **(D)** Confocal micrographs of NIH3T3 cells incubated with mitotracker (red) and transfected with Gα_q-N-terminus (1–124 aa) GFP and Flag, immunostained with anti-Flag and mounted with DAPI. MEF cells transiently expressing Gα_q IE25/26AA mutants incubated with mitotracker (red), immunostained with anti-G$\alpha_{q/11}$ and mounted with DAPI. Line profile was generated by LAS AF.

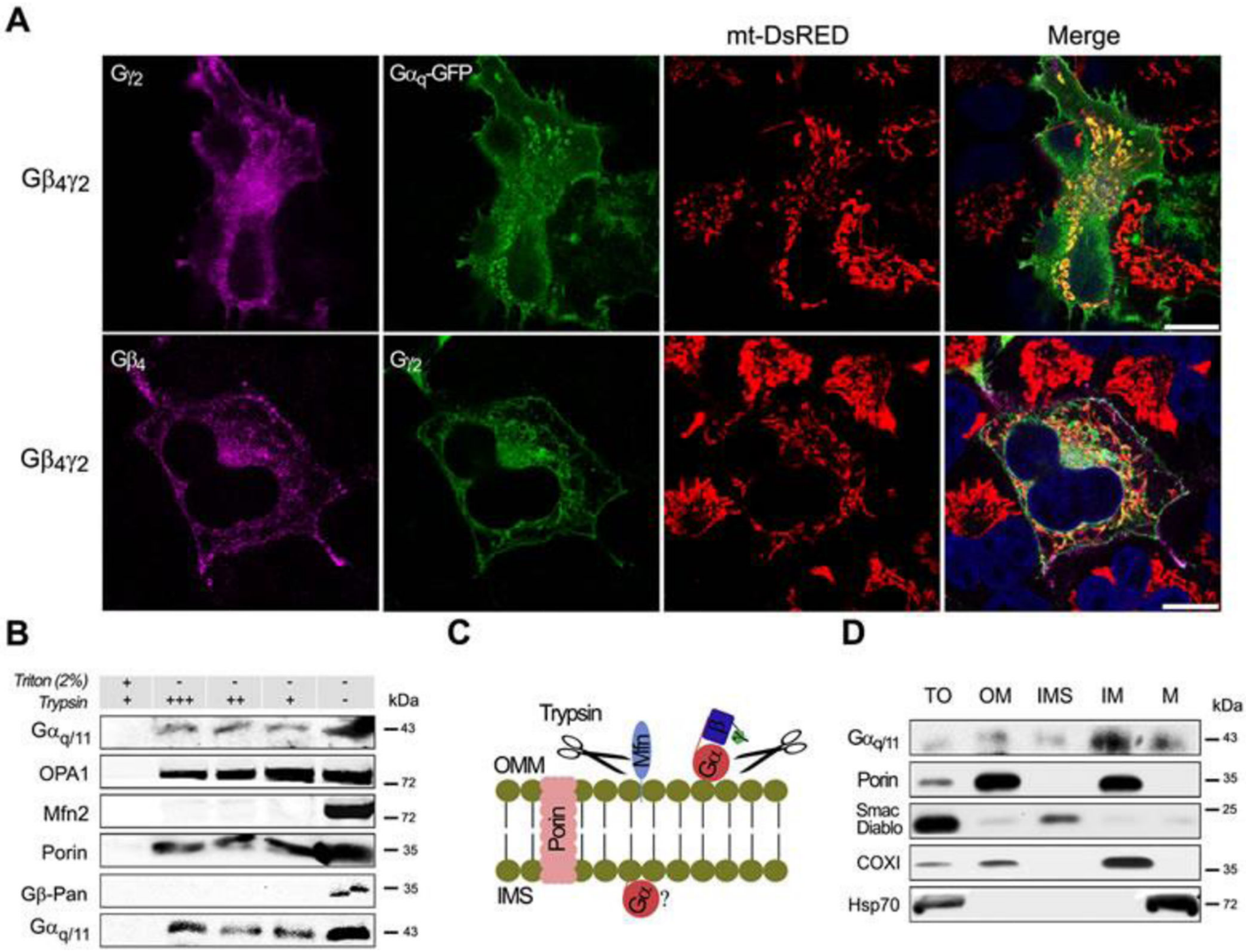

Fig. 2. Gα_q and different G$\beta\gamma$ dimers localized at the mitochondria

(A) Confocal micrographs of HeLa cells stably expressing mt-DsRed and Gβ4-Flag γ2-HA and/or Gα_q, immunostained with anti-Flag or HA and mounted with DAPI. **(B)** Mitochondrial fractions of NIH3T3 cells submitted to trypsin digestion in presence or absence of Triton X-100, immunoblotted with anti-G$\alpha_{q/11}$, OPA1 (inner membrane), Mfn2 (outer membrane), Porin (integral outer membrane) and Gβ-Pan (representing Gβγ dimer). **(C)** Diagram showing the likely actions of trypsin on proteins blotted in B. **(D)** Mouse liver mitochondrial sub-fractions shown the presence of G$\alpha_{q/11}$ at the inner membrane, immunoblotted with G$\alpha_{q/11}$ and markers: Porin (OM), Smac/Diablo (IMS), COXI (IM) and Hsp70 (M).

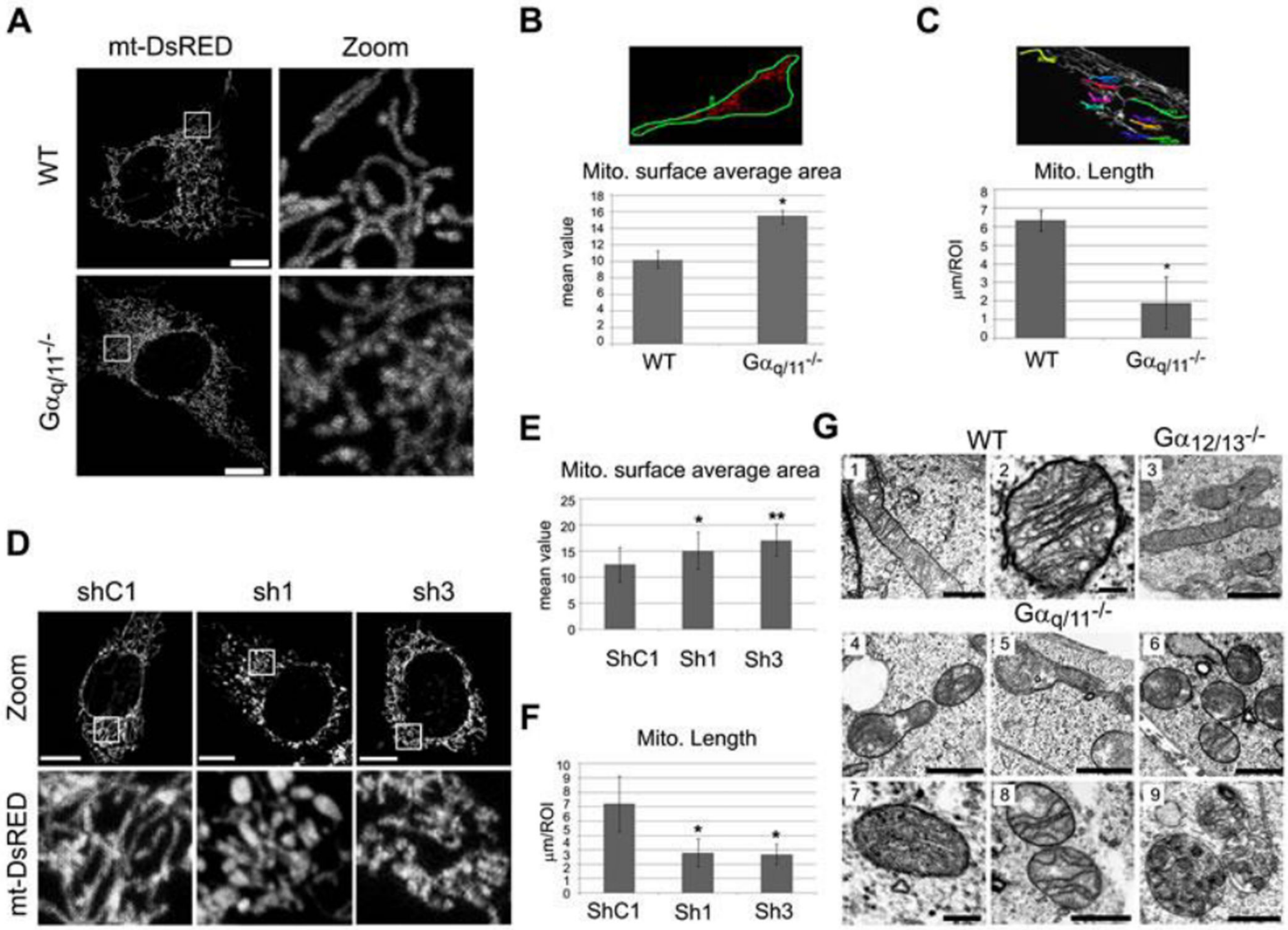

Fig. 3. MEF G$\alpha_{q/11}$ knockout (G$\alpha_{q/11}^{-/-}$) and shRNA depleted cells show alterations of the mitochondrial network and morphology

(A) Representative confocal micrographs of MEF wild-type (WT) and G$\alpha_{q/11}^{-/-}$ cells expressing the mitochondrial matrix-targeted mt-DsRed after 24 h of transfection. **(B)** Mitochondrial surface average area calculated by the Polygon ROI with LAS AF software. The mean value of different intensities inside the ROI is related to the distribution of the fluorochrome. Data represent mean ± s.d. (n=45). Mann-Whitney test was employed (*p<0.0001). Experiments were carried out as in A. **(C)** Mitochondria length was calculated by the polyline measurement. Data represent mean ± s.d. (n=25) for 10 ROIs each. Mann-Whitney test was utilized (*p<0.0001). Experiments were carried out as in A. **(D)** Representative confocal micrographs of MEF wild-type cells infected by a lentivirus containing two different sequences of shRNA (1 and 3) against G$\alpha_{q/11}$ and one control shRNA (shC1) expressing mt-DsRed protein after 24 h of transfection. **(E)** Experiments were carried out as in D and calculated as in B. Data represent mean ± s.d. (n=25). Student's t-test was employed (*p=0.0063 and **p<0.001). **(F)** Experiments were carried out as in D and calculated as in C. Data represent mean ± s.d. (n=25). Kruskal-Wallis test was utilized (*p<0.0001). **(G)** TEM micrographs showing the mitochondrial ultrastructure of MEFs WT

(1–2), $G\alpha_{q/11}^{-/-}$ (4–9) and $G\alpha_{12/13}^{-/-}$ (3) cells. Scale bars: 0.5 µm and 0.1 µm in 2. See also Figure S3C for more micrographs of $G\alpha_{12/13}^{-/-}$ cells.

Author Manuscript
Author Manuscript
Author Manuscript

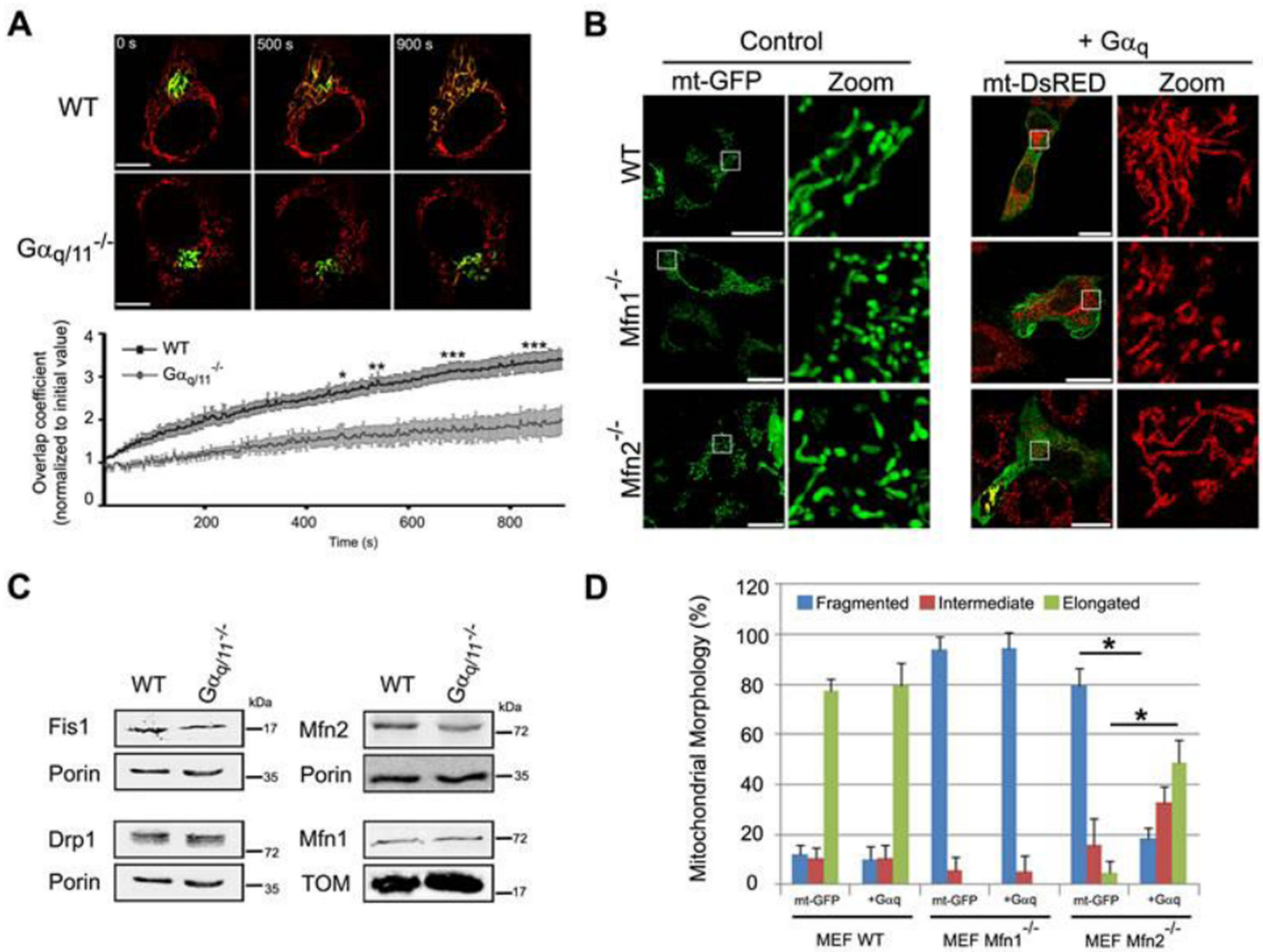

Fig. 4. Impairment in mitochondria fusion in absence of $G\alpha_{q/11}$

(A) MEFs transfected with mt-DsRed and mito-PAGFP. Mito-PAGFP was photoactivated, mt-DsRed was photobleached at t=0 s. Panels show the same cell at a range of time points. Scale bar: 75 µm. Data show mean ± s.e.m (n=5). ANOVA (*p<0.05, **p<0.01 and ***p<0.001) was employed. **(B)** Confocal micrographs of MEFs transfected with mt-GFP or $G\alpha_q$/mt-DsRED, immunostained with anti-$G\alpha_{q/11}$ antibody (right panel in green). Zoom shows only mitochondria. Scale bar: 25 µm. **(C)** Mitochondrial morphology was scored from B. Data represent mean ± s.d. (n=50) of three independent experiments. Chi-Square test was employed (*p<0.0001). **(D)** Confocal micrographs of MEFs in presence of Gβ2-Flag (green on left and purple on right panel)/mt-dsRED with or without $G\alpha_q$-GFP (green on right panel) mounted with DAPI (blue). Zoom shows only mitochondria.

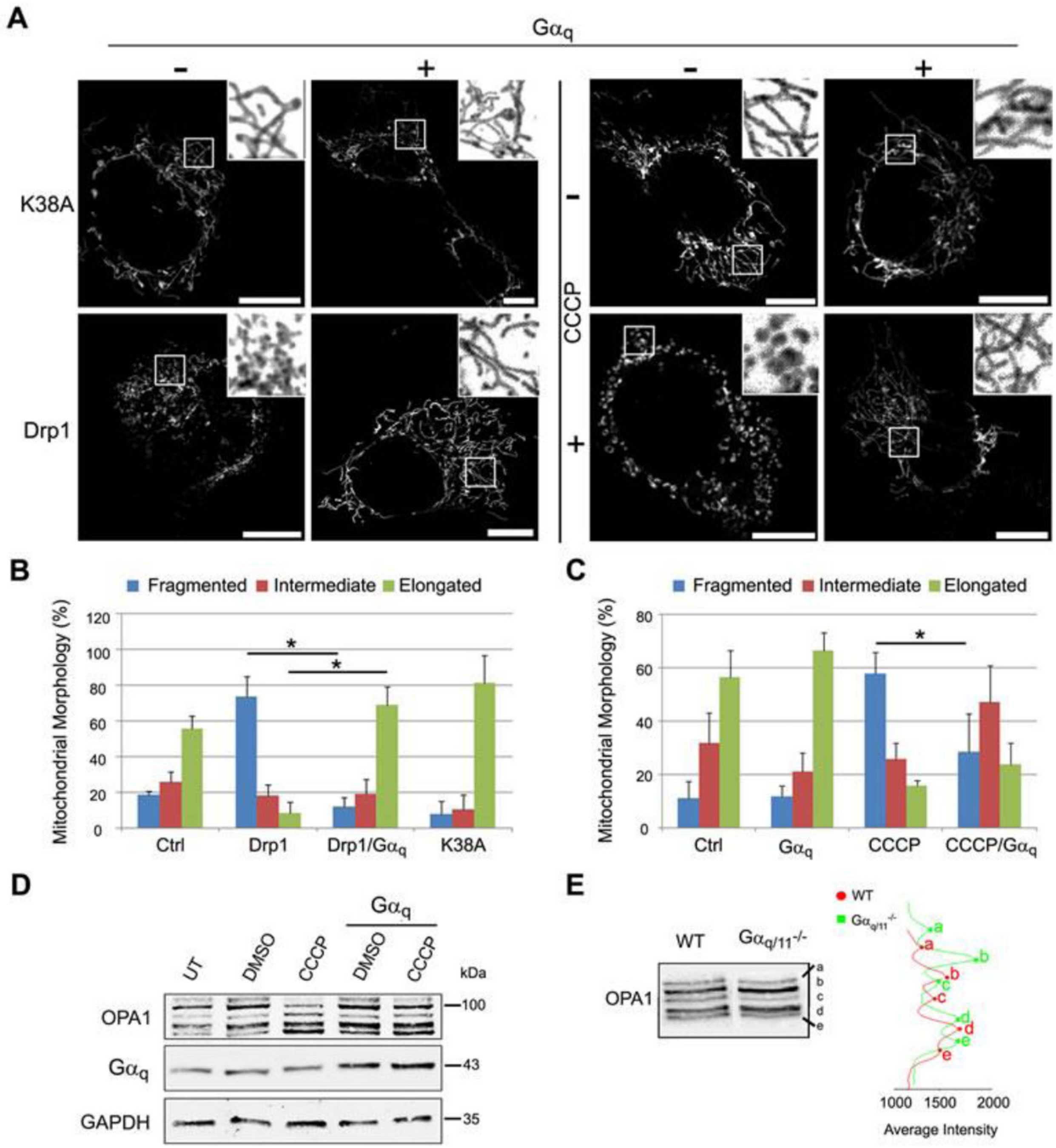

Fig. 5. Gα$_q$ stabilizes mitochondrial fusion, blocking fragmentation induced by Drp1 or CCCP

(A) Confocal micrographs of MEF wild-type cells transfected with mt-DsRed (grey) and Drp1-HA or Drp1-(K38A)-HA or treated with 10 μM CCCP (+) or DMSO (−) for 3h, overexpressing (+) or not (−) Gα$_q$, immunostained with anti-HA and anti-Gα$_{q/11}$ (not shown). **(B-C)** Mitochondrial morphology quantified as mentioned in Figure 4C. Chi-Square test was employed (*p<0.0001). Experiments were carried out as in A. Data represent mean ± s.d. (n=50) of three independent experiments. **(D)** MEF cells were transfected with pcDNA3 or pcDNA3-Gα$_q$ and the day after incubated for 3h with 10 μM CCCP or DMSO.

Lysates were immunoblotted with the indicated antibodies. **(E)** MEF WT and G$\alpha_{q/11}{}^{-/-}$ cells immunoprecipitated for OPA1 isoforms and immunoblotted with OPA1 antibody, quantified by Line Profile of Odyssey System.

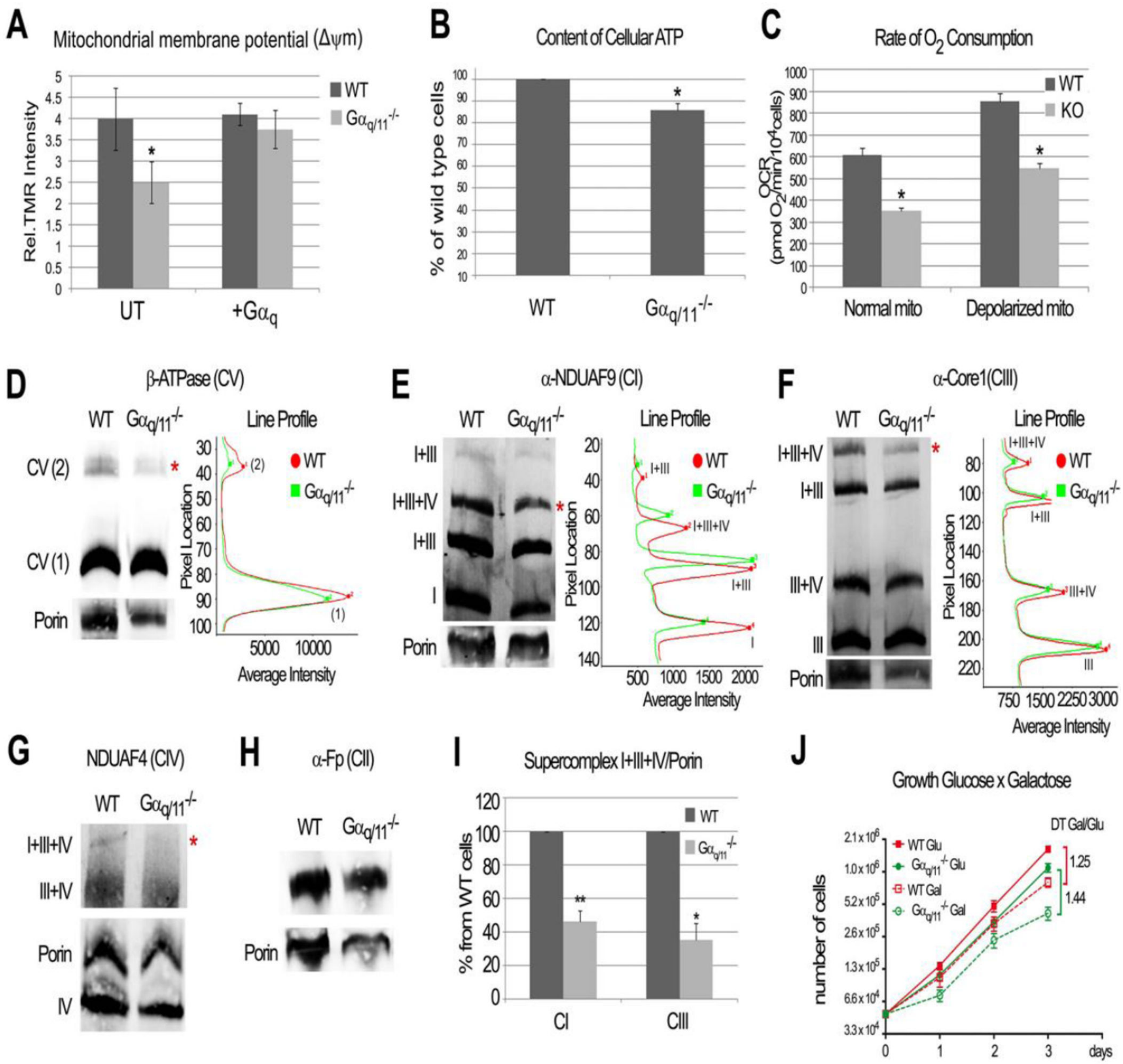

Fig. 6. Gα$_{q/11}$ are needed for normal mitochondrial function and respiratory supercomplexes assembly

(A) MEF Gα$_{q/11}^{-/-}$ cells show decreased mitochondrial membrane potential (ΔΨm). + Gα$_q$ indicates that cells were transfected with pcDNA3-Gα$_q$ the day before analysis. Data represent mean ± s.d. (n=4 WT and n=6 KO). Unpaired t-test was employed (*p=0.0023). **(B)** Decreased content of cellular ATP is observed in Gα$_{q/11}^{-/-}$ cells. Data represent mean ± s.d. (n=4) with normalized values respect to WT (%). Paired t-test (*p=0.0014) was utilized. **(C)** Gα$_{q/11}^{-/-}$ cells present less oxygen consumption (OCRs) rate. After baseline measurements (normal mito) cells were depolarized (CCCP). Data represent mean ± s.e.m (n=18 WT and n=20 KO). Unpaired t-test (*p<0.0001) was employed. **(D-H)** Mitochondria from MEFs were lysed in digitonin and resolved by BN-PAGE then blotted to determine native complexes and supercomplexes: **(D)** Complex V (β-ATPase); **(E)** Complex I (detected by α-NDUFA9); **(F)** Complex III (α-Core1); **(G)** complex IV (NDUFA4) and **(H)** complex II (α-Fp). **(I)** Ratio of supercomplexes I+III+IV per Porin, quantified by Odyssey System utilizing experiments from E and F. Data represent mean ± s.d. (n=5 CI and n=3 CIII). Paired t-test (**p<0.0001, * p<0.01) was utilized. * denotes changes in supercomplex band intensity. **(J)** Cells growth in glucose (Glu) *versus* galactose (Gal) per days and doubling time (DT) ratio. Statistical significance was found by one-way ANOVA followed by Tukey´s test after day 2 in both conditions for KO compared to WT cells (p<0.05). Data represent mean ± s.e.m (n=6).

Accession	Coverage	# PSMs	# Peptides	# AAs	MW [kDa]	calc. pI	Score	Description
P05202	79.77	291	43	430	47.4	9.00	886.47	Aspartate aminotransferase, mitochondrial OS=Mus musculus GN=Got2 PE=1 SV=1 - [AATM_MOUSE]
Q9QYA2	78.95	60	20	361	37.9	7.74	203.62	Mitochondrial import receptor subunit TOM40 homolog OS=Mus musculus GN=Tomm40 PE=1 SV=3 - [TOM40_MOUSE]
Q99JB2	80.17	54	29	353	38.4	8.87	178.95	Stomatin-like protein 2 OS=Mus musculus GN=Stoml2 PE=1 SV=1 - [STML2_MOUSE]
P05064	83.52	58	30	364	39.3	8.09	170.75	Fructose-bisphosphate aldolase A OS=Mus musculus GN=Aldoa PE=1 SV=2 - [ALDOA_MOUSE]
P08752	57.75	46	26	355	40.4	5.45	140.70	Guanine nucleotide-binding protein G(i) subunit alpha-2 OS=Mus musculus GN=Gnai2 PE=1 SV=4 - [GNAI2_MOUSE]
Q9DC51	72.32	50	28	354	40.5	5.69	138.03	Guanine nucleotide-binding protein G(k) subunit alpha OS=Mus musculus GN=Gnai3 PE=1 SV=3 - [GNAI3_MOUSE]
Q9ER88	68.29	48	25	391	44.7	8.94	128.17	28S ribosomal protein S29, mitochondrial OS=Mus musculus GN=Dap3 PE=2 SV=1 - [RT29_MOUSE]
Q9D6R2	53.83	46	25	366	39.6	6.73	117.94	Isocitrate dehydrogenase [NAD] subunit alpha, mitochondrial OS=Mus musculus GN=Idh3a PE=1 SV=1 - [IDH3A_MOUSE]
Q9DBL1	49.77	34	21	432	47.8	7.87	115.01	Short/branched chain specific acyl-CoA dehydrogenase, mitochondrial OS=Mus musculus GN=Acadsb PE=1 SV=1 - [ACDSB_MOUSE]
Q07417	59.22	34	24	412	44.9	8.79	106.53	Short-chain specific acyl-CoA dehydrogenase, mitochondrial OS=Mus musculus GN=Acads PE=2 SV=1 - [ACADS_MOUSE]
Q9CXW2	63.23	37	23	359	41.2	8.56	91.61	28S ribosomal protein S22, mitochondrial OS=Mus musculus GN=Mrps22 PE=2 SV=1 - [RT22_MOUSE]
Q99K85	59.73	28	19	370	40.4	8.03	87.01	Phosphoserine aminotransferase OS=Mus musculus GN=Psat1 PE=1 SV=1 - [SERC_MOUSE]
Q99KV1	39.39	25	16	358	40.5	6.32	79.85	DnaJ homolog subfamily B member 11 OS=Mus musculus GN=Dnajb11 PE=1 SV=1 - [DJB11_MOUSE]
Q8BGC4	48.54	22	15	377	40.5	7.42	77.43	Zinc-binding alcohol dehydrogenase domain-containing protein 2 OS=Mus musculus GN=Zadh2 PE=2 SV=1 - [ZADH2_MOUSE]
O35855	44.53	24	16	393	44.1	8.29	72.26	Branched-chain-amino-acid aminotransferase, mitochondrial OS=Mus musculus GN=Bcat2 PE=2 SV=2 - [BCAT2_MOUSE]
Q8QZS1	55.32	21	17	385	43.0	8.06	71.64	3-hydroxyisobutyryl-CoA hydrolase, mitochondrial OS=Mus musculus GN=Hibch PE=1 SV=1 - [HIBCH_MOUSE]
Q920E5	43.63	23	15	353	40.6	5.66	69.44	Farnesyl pyrophosphate synthase OS=Mus musculus GN=Fdps PE=2 SV=1 - [FPPS_MOUSE]
Q921H8	45.99	24	15	424	43.9	8.44	68.46	3-ketoacyl-CoA thiolase A, peroxisomal OS=Mus musculus GN=Acaa1a PE=2 SV=1 - [THIKA_MOUSE]
Q91ZE0	46.08	23	15	421	49.6	8.25	67.29	Trimethyllysine dioxygenase, mitochondrial OS=Mus musculus GN=Tmlhe PE=2 SV=2 - [TMLH_MOUSE]
P18872	44.63	22	14	354	40.1	5.53	63.74	Guanine nucleotide-binding protein G(o) subunit alpha OS=Mus musculus GN=Gnao1 PE=1 SV=3 - [GNAO_MOUSE]

Accession	Coverage	# PSMs	# Peptides	# AAs	MW [kDa]	calc. pI	Score	Description
Q99N87	38.66	23	18	432	48.2	10.14	61.98	28S ribosomal protein S5, mitochondrial OS=Mus musculus GN=Mrps5 PE=2 SV=1 - [RT05_MOUSE]
Q99LC3	48.45	23	17	355	40.6	7.78	60.83	NADH dehydrogenase [ubiquinone] 1 alpha subcomplex subunit 10, mitochondrial OS=Mus musculus GN=Ndufa10 PE=1 SV=1
Q9WUR2	41.69	15	12	391	43.2	8.92	58.98	Peroxisomal 3,2-trans-enoyl-CoA isomerase OS=Mus musculus GN=Peci PE=1 SV=2 - [PECI_MOUSE]
P21278	38.16	21	15	359	42.0	5.97	57.17	Guanine nucleotide-binding protein subunit alpha-11 OS=Mus musculus GN=Gna11 PE=1 SV=1 - [GNA11_MOUSE]
Q9Z1G3	45.03	20	16	382	43.9	7.46	56.37	V-type proton ATPase subunit C 1 OS=Mus musculus GN=Atp6v1c1 PE=1 SV=4 - [VATC1_MOUSE]
Q8R3F5	36.75	18	12	381	41.9	8.10	54.81	Malonyl-CoA-acyl carrier protein transacylase, mitochondrial OS=Mus musculus GN=Mcat PE=2 SV=3 - [FABD_MOUSE]
P22315	49.29	20	18	420	47.1	8.91	53.50	Ferrochelatase, mitochondrial OS=Mus musculus GN=Fech PE=1 SV=2 - [HEMH_MOUSE]
Q8BGA9	27.25	19	11	433	48.2	9.61	50.72	Mitochondrial inner membrane protein OXA1L OS=Mus musculus GN=Oxa1l PE=2 SV=1 - [OXA1L_MOUSE]
P21279	31.20	17	13	359	42.1	5.68	48.91	Guanine nucleotide-binding protein G(q) subunit alpha OS=Mus musculus GN=Gnaq PE=1 SV=4 - [GNAQ_MOUSE]
Q8K2M0	40.53	20	15	380	45.0	8.10	44.52	39S ribosomal protein L38, mitochondrial OS=Mus musculus GN=Mrpl38 PE=2 SV=2 - [RM38_MOUSE]
Q8QZT1	37.03	16	13	424	44.8	8.51	43.10	Acetyl-CoA acetyltransferase, mitochondrial OS=Mus musculus GN=Acat1 PE=1 SV=1 - [THIL_MOUSE]
Q91V12	34.91	16	13	381	42.5	8.68	41.86	Cytosolic acyl coenzyme A thioester hydrolase OS=Mus musculus GN=Acot7 PE=1 SV=2 - [BACH_MOUSE]
P08249	40.24	12	10	338	35.6	8.68	41.13	Malate dehydrogenase, mitochondrial OS=Mus musculus GN=Mdh2 PE=1 SV=3 - [MDHM_MOUSE]
Q99M04	46.11	15	13	373	41.9	8.88	40.91	Lipoyl synthase, mitochondrial OS=Mus musculus GN=Lias PE=2 SV=1 - [LIAS_MOUSE]
P10605	35.99	12	11	339	37.3	5.91	39.06	Cathepsin B OS=Mus musculus GN=Ctsb PE=1 SV=2 - [CATB_MOUSE]
P56480	29.49	11	9	529	56.3	5.34	38.90	ATP synthase subunit beta, mitochondrial OS=Mus musculus GN=Atp5b PE=1 SV=2 - [ATPB_MOUSE]
Q9D8V0	36.24	14	10	378	41.7	6.04	38.79	Minor histocompatibility antigen H13 OS=Mus musculus GN=Hm13 PE=1 SV=1 - [HM13_MOUSE]
O89017	20.69	11	7	435	49.3	6.39	36.39	Legumain OS=Mus musculus GN=Lgmn PE=1 SV=1 - [LGMN_MOUSE]
Q8JZM0	44.06	13	12	345	38.9	9.47	35.31	Dimethyladenosine transferase 1, mitochondrial OS=Mus musculus GN=Tfb1m PE=2 SV=1 - [TFB1M_MOUSE]
O09174	41.21	12	11	381	41.7	7.40	34.86	Alpha-methylacyl-CoA racemase OS=Mus musculus GN=Amacr PE=1 SV=3 - [AMACR_MOUSE]
Q9CR16	27.03	11	9	370	40.7	7.43	34.80	Peptidyl-prolyl cis-trans isomerase D OS=Mus musculus GN=Ppid PE=1 SV=3 - [PPID_MOUSE]

Accession	Coverage	# PSMs	# Peptides	# AAs	MW [kDa]	calc. pI	Score	Description
Q9D7B6	28.57	14	12	413	45.0	8.13	34.16	Isobutyryl-CoA dehydrogenase, mitochondrial OS=Mus musculus GN=Acad8 PE=2 SV=2 - [ACAD8_MOUSE]
Q3URS9	34.24	11	9	406	45.1	8.09	33.59	Coiled-coil domain-containing protein 51 OS=Mus musculus GN=Ccdc51 PE=2 SV=1 - [CCD51_MOUSE]
Q924D0	27.78	10	9	396	43.3	9.20	33.23	Reticulon-4-interacting protein 1, mitochondrial OS=Mus musculus GN=Rtn4ip1 PE=1 SV=2 - [RT4I1_MOUSE]
Q99JY4	34.04	15	11	376	42.2	8.41	32.73	TraB domain-containing protein OS=Mus musculus GN=Trabd PE=2 SV=1 - [TRABD_MOUSE]
Q8VCM4	26.01	10	9	373	42.1	8.48	32.70	Lipoyltransferase 1, mitochondrial OS=Mus musculus GN=Lipt1 PE=2 SV=1 - [LIPT_MOUSE]
O35435	53.42	13	13	395	42.7	9.55	32.01	Dihydroorotate dehydrogenase, mitochondrial OS=Mus musculus GN=Dhodh PE=2 SV=2 - [PYRD_MOUSE]
Q91WK2	26.99	9	8	352	39.8	6.67	29.85	Eukaryotic translation initiation factor 3 subunit H OS=Mus musculus GN=Eif3h PE=1 SV=1 - [EIF3H_MOUSE]
P63085	35.47	10	8	358	41.2	6.98	28.75	Mitogen-activated protein kinase 1 OS=Mus musculus GN=Mapk1 PE=1 SV=3 - [MK01_MOUSE]
Q8BVU5	36.00	14	12	350	38.6	6.76	28.43	ADP-ribose pyrophosphatase, mitochondrial OS=Mus musculus GN=Nudt9 PE=2 SV=1 - [NUDT9_MOUSE]
Q8R0Z5	26.92	8	8	364	39.3	8.44	28.15	Mitoferrin-2 OS=Mus musculus GN=Slc25a28 PE=2 SV=1 - [MFRN2_MOUSE]
Q9CZ57	32.02	12	11	381	42.8	8.25	27.90	Putative methyltransferase NSUN4 OS=Mus musculus GN=Nsun4 PE=2 SV=1 - [NSUN4_MOUSE]
Q99M87	21.25	12	9	480	52.4	9.22	27.51	DnaJ homolog subfamily A member 3, mitochondrial OS=Mus musculus GN=Dnaja3 PE=1 SV=1 - [DNJA3_MOUSE]
Q8R0G7	22.16	6	5	528	56.7	7.15	27.12	Protein spinster homolog 1 OS=Mus musculus GN=Spns1 PE=2 SV=1 - [SPNS1_MOUSE]
Q8CAY6	31.23	9	7	397	41.3	7.50	26.23	Acetyl-CoA acetyltransferase, cytosolic OS=Mus musculus GN=Acat2 PE=1 SV=2 - [THIC_MOUSE]
Q791T5	31.36	12	11	389	41.5	9.32	26.19	Mitochondrial carrier homolog 1 OS=Mus musculus GN=Mtch1 PE=1 SV=1 - [MTCH1_MOUSE]